Evaluation of Mechanical Properties of Porous 6061 Alloys Fabricated by the Powder Compression and Induction Heating Process

S.W. YOUN and C.G. KANG

The purpose of this study is to evaluate the mechanical properties of 6061 Al foam products, which were fabricated by the powder compression and multistep induction heating method, and to build the database necessary for computer-aided modeling or foam components design. In this study, 6061 Al foams with various porosity fractions were fabricated according to the porosity fractions–final heating temperature curve. The relationships between porosity fraction and morphological properties (porosity diameter, number per unit area of porosities, and surface skin thickness) were investigated. Mechanical properties such as compressive strength, energy absorption capacity, and efficiency were investigated to evaluate the feasibility of foams as crash-energy-absorbing components. Furthermore, the effect of the surface skin thickness on the plateau stress and strain sensitivity of the 6061 Al foam with low porosities (pct) was studied.

I. INTRODUCTION

ALUMINUM foam is an ultra-lightweight porous material consisting of aluminum and large quantities of porosities. It has high stiffness at very low density, high impact energy absorption, heat and fire resistance, and greater thermal stability than any organic material.[1,2] One of the advantages of foam material is that the material with required mechanical properties can be produced by controlling the porosities. In spite of the advantages mentioned previously, Al foam is hardly used in the industry. One reason is the difficulty of reproducing mechanical properties. In order to use foamed metal as a tailored material in the industry, the following points need to be investigated. One is the relationship between morphological and mechanical properties; another is the fabrication condition for Al foam, which satisfies the desired morphological properties. In addition, for the purpose of a finite- element analysis, the establishment of a data base of mechanical properties is essential. One of the most important application fields for Al foam in general is energy absorption, because of Al foam's low rebound in dynamic crash situations and much higher strength than polymer foam. Generally, foamed metal has a porosity fraction that ranges approximately from 70 to 90 pct, because the greater a metal's porosity, the greater its usable strain as an energy absorber.[3] Therefore, so far, studies on the mechanical properties of foamed metal have been conducted mainly on metals with porosity fractions greater than 70 pct. Wan and colleagues have researched the deformation behavior of foamed material and the energy absorption rate in accordance with the variation of porosity fraction through a compression experiment on AlSi7Mg0.45 alloys with porosity fractions of 75 to 85 pct.[4] Yu *et al*. have reported that compressive strength of A6061 alloys with porosities of 70 to 90 pct is dominated by relative density and is not affected significantly by the variation of strain rate.[5] However, a sandwich type of foam product that is united with high-strength materials is widely used, because the higher the porosity fraction of a foam, the greater the energy absorption efficiency and the less the compression intensity.[6] In the case of three-dimensional foam products with a complex shape, bonding with other materials is not feasible. It is also expected that a data base of the mechanical properties of foamed metal with porosity fractions below 70 pct will need to be established to be useful in tailoring materials.

Additionally, the surface skin that is inevitably generated in producing Al foam product has a strong influence on mechanical properties. It has been reported that the presence of the surface skin significantly improves the compressive strength and results in a more constant and homogeneous plateau stress compared to the case without surface skin, although the apparent density is almost equal.[7,8] However, there is still little research on the effect of the surface skin thickness on mechanical properties.

In this study, 6061 Al foams with various porosity fractions (P_f) were fabricated according to the porosity fractions' (P_f) final heating temperature (T_{a3}) curves. The relationships between P_f and morphological properties (porosity diameter [D_e], number per unit area of porosities [N_p], and surface skin thickness [t_s]) were investigated. Mechanical properties such as compressive strength, energy absorption capacity, and efficiency were investigated to evaluate the feasibility of foams as crash-energy-absorbing components. Furthermore, the effect of the surface skin thickness on the plateau stress and strain sensitivity of the 6061 Al foam with low porosities (53, 59, and 66 pct) was studied.

II. FABRICATION OF Al FOAM WITH VARIOUS POROSITIES FOR COMPRESSION TESTS

In order to measure the mechanical properties of 6061 Al foam material, a uniaxial compression experiment was conducted. The Al foam specimens for the compression experiment were produced by the powder metallurgy and multistep induction heating method. Powdered Al 6061 (325 mesh) alloy and TiH_2

S.W. YOUN, Research Assistant, Department of Precision and Mechanical Engineering, and C.G. KANG, Professor, School of Mechanical Engineering, are with Pusan National University, P/Busan, 609-735, South Korea. Contact e-mail: yswonny@pusan.ac.kr or cgkang@pusan.ac.kr

Manuscript submitted August 26, 2003.

powder (200 mesh) were used as the matrix alloy and foaming agent, respectively. Table I shows the chemical composition of the 6061 Al alloy, and Figures 1 and 2 show the process layout and equipment for Al foam fabrication. The measurements, sizes, and manufacturer of the equipment used in the experiment are shown in Tables II and III.

After the 6061 Al alloy powder (30 g) and TiH_2 powder (0.3 wt pct) were mixed using a V mixer at the speed of 30 rpm, the mixed powder was put into the compression die cavity and preheated to $T_{pre} = 450$ °C at an output of 6 kW using an induction heating device. The preheating temperature of the mixed powder was determined according to the result of a thermogravimetric analysis.[9] In the temperature range of 500 °C to 600 °C, a remarkable weight loss of TiH_2 occurred due to a thermal decomposition reaction of the TiH_2. Therefore, the preheating temperature of the mixed powder must be set below 500 °C to reduce the loss of H_2 gas. In addition, heat treating the hydride in air, to temperatures between roughly 400 °C and 500 °C, has been reported to delay the decomposition of TiH_2 and been found to be effective when adding TiH_2 to molten metals.[10,11] Two K-type CA thermocouples (o.d. 1.6) were used to measure the temperature of the center and the upper part of the powder. If the preheated mixed powder is cooled immediately after the hot press with an upper punch, the foamable precursor contracts to the size of 30-mm diameter × 14-mm height.

Residual porosity that remains inside of the precursor interferes with the uniform growth of porosities as it increases the passage of H_2 gas in foaming.[12] Therefore, to produce a precursor void of residual porosity, the mixed powder was compressed with an applied pressure of 120 kN after preheating to the temperature of 450 °C.[13]

For the foaming experiment, a mold divided into left and right sides and made of stainless steel was used, and to precisely control the temperature of the precursor, the temperature in the center of the lower part of the precursor was measured using a K-type CA thermocouple (Figure 1). The produced foamable precursor ($d \times h = 31 \times 14$ mm) was foamed using the multistep induction heating process. Figure 3 and Table IV shows the heating conditions and the input-data diagram of multistep induction heating, respectively. 6061 Al foam specimens with various porosity fractions were produced for a variation of the final heating temperature (T_{a3}) according to the T_{a3}-porosity fraction (pct) curve of Figure 4 that was measured experimentally.[13]

Figure 5 shows the 6061 Al foam specimens that were fabricated in this study. No heat treatment was performed after foaming. A well-conditioned, flawless surface appearance can be observed. In order to measure the porosity fraction (P_f), porosity size (D_e), number per unit area (N_p), and surface skin thickness of the specimens, an image analysis on a cross section of the foaming direction was conducted with an image

Table I. Chemical Composition of Powdered 6061 Al Alloy

Cr	Cu	Fe	Mg	Mn	Si	Ti	V	Pct Al
0.07	0.25	0.25	0.89	0.03	0.65	0.02	0.01	bal

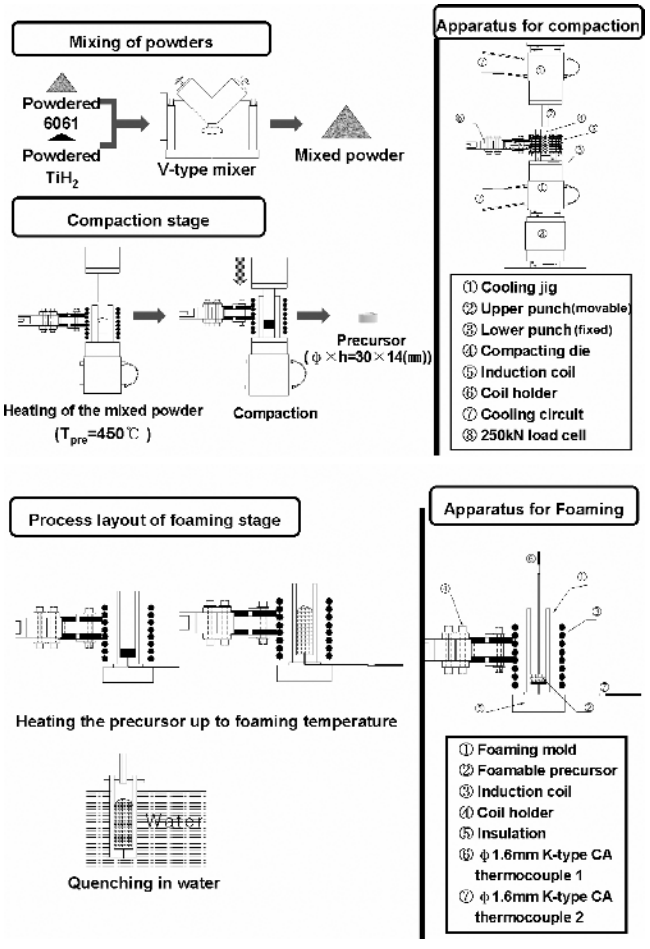

Fig. 1—Process layout of 6061 Al foam fabrication.

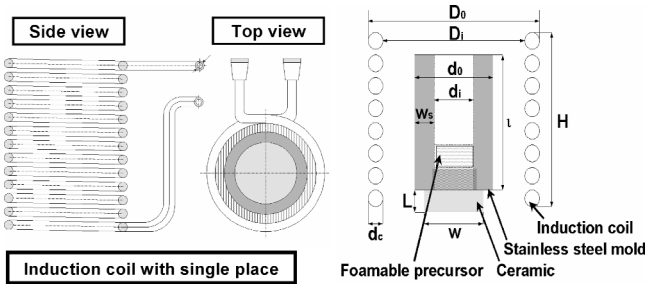

Fig. 2—Schematic diagram of induction heating device.

Table II. Specifications of Equipment for Experiment

Compaction and Compression Test	Material Testing System, Maximum Load 250 kN, 1300 °C (MTS, MN, USA)
Heating (foaming)	induction heating system 25 kW, 40 kHz, (solid Industrial Co., Busan, Korea)

Table III. Dimensions of Induction Heating Device (unit: mm)

Coil Inner Diameter (D_i)	Mold Inner Diameter (d_0)	Mold Outer Diameter (d_j)	Coupling Distance (W_s)
80	30	70	10
Coil Length (H)	Mold Length (l)	Coil Wall Thickness (d_c)	—
150	130	10	—

analyzer (Leica M/W, Leica Microsystems Imaging Solutions, Ltd., Cambridge, U.K.). Since the shapes of porosities were not perfect circles, equivalent diameter (D_e) is used for noting the porosity size. An equivalent diameter is the diameter of a circle having the same area as the porosities, which was calculated automatically by image analyzer. For image analysis, the cross-sectional surfaces of specimens were sprayed with graphite (black color) instead of black resin. A compression test specimen was machined with the size of $d \times H = 31 \times 25$ mm, and the surface skin that is inevitably generated in the process of the production of Al foam was retained. The surface skin is not generally eliminated as it significantly enhances mechanical properties such as compression strength and the plateau stress of Al foam components. In the preparation of the specimen, the following two facts were considered. One fact is that the minimum dimension of the specimen should be at least 7 times the porosity size to avoid porosity size effect, and another is that the smaller the specimens the closer the apparent mass density corresponds to the local mass density.[6] Compression experiments were performed using the MTS at a crosshead speed of 0.25 mm/s (0.01 s^{-1}). During the compression experiment, the strain rate was changed by the speed control of the compression punch. The strain rate is defined as $\varepsilon = V_p/H_0$, where V_p and H_0 show the punch speed and the initial height of the specimen, respectively.

III. MECHANICAL PROPERTIES OF Al FOAM WITH VARIOUS POROSITIES

A. *Variation of Stress-Strain Curves with Variation in Porosities*

Figure 6 shows the relationship between porosity fractions (P_f) and morphological properties such as porosity diameter (D_e), number per unit area of porosities (N_p), and surface skin thickness (t_s). Figure 6(a) shows the relationship between porosity fractions and porosity size. The porosity size increases with increasing porosity fractions due to both growth and coalescence of porosities. The occurrence of the coalescence of the porosities can be confirmed in that the number of porosities decreased, as shown in Figure 6(b). Figure 6(c) shows the relationship between porosity fractions and surface skin thickness. Even though the porosity fractions, porosity size, and porosity number remarkably changed, the surface skin thickness did not change. Over the $P_f = 48$ to 72 pct range, the t_s was maintained at about 0.4 to 0.6 mm. However, in the case of $P_f = 76$ pct, the t_s range remarkably increased to 0.3 to 1.1 mm.

Figure 7 shows the stress-strain curve of the 6061 Al foam material with different porosity fractions. The specimens were tested without any further heat treatment after foaming. During the compression experiment, bending and buckling of porosities occurred, and a stress-strain curve with no fluctuations was obtained because wrought Al alloy material was used as a matrix alloy. On the other hand, when using a cast alloy as the matrix alloy, it has been reported that the stress fluctuation increases with increasing strain as fracture is the dominant mechanism instead of bending and buckling of the porosity during compression experiments.[14] As a whole, from Figures 7(a) through (f), it can be seen that a compression strength rise in consistent with a decrease of fraction of porosity and usable strain as an energy absorber; in other words, the plateau stress region decreases. An ideal energy absorber keeps the stress condition regular, and, at the same time, plastic deformation is proceded. This strain is called a plateau strain. Theoretically, metallic foam simultaneously generates plastic deformation and buckling or fractures of cell walls during the compression test. Therefore, deformation behavior in which strain is preceded without stress increases after yield point is shown. However, as can be seen from Figure 7, stress increases slowly in accordance with the strain increase after the yield point. With the decrease of the porosity fraction, the plateau stress region in the stress-strain curve decreases. This is due to the fact that as the porosity fraction

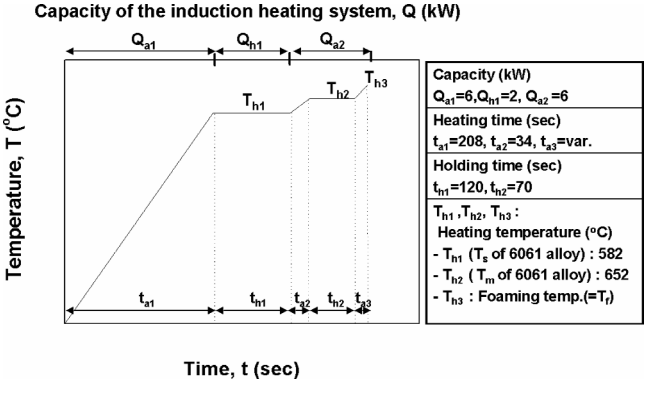

Fig. 3—Proposed input data diagram of multistep induction heating.

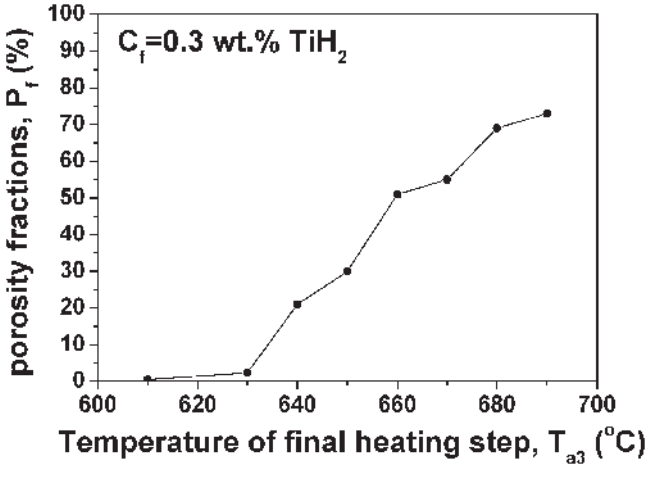

Fig. 4—Relationship between temperature of final heating step (T_{a3}) and porosity fractions (pct).[11]

Table IV. Input-Data of Multistep Induction Heating

	Heating Time t_a (s)			Heating temperature T_a (°C)			Holding Time t_h (s)		
Mold	t_{a1}	t_{a2}	t_{a3}	T_{a1}	T_{a2}	$T_{a3} = T_f$	t_{h1}	t_{h2}	t_{h3}
304 SS	208	34	variation	590	640	variation	120	70	without

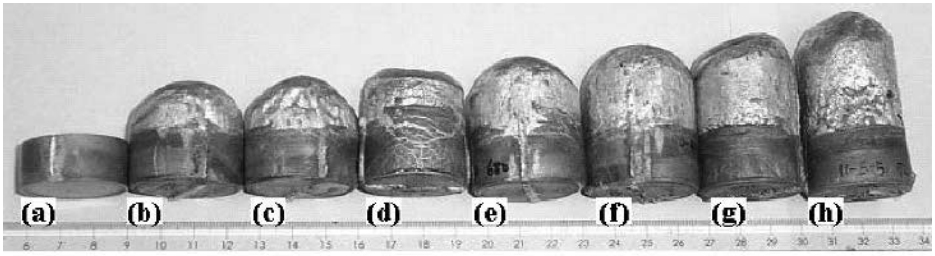

(a) Surface appearances of 6061 Al foam specimens

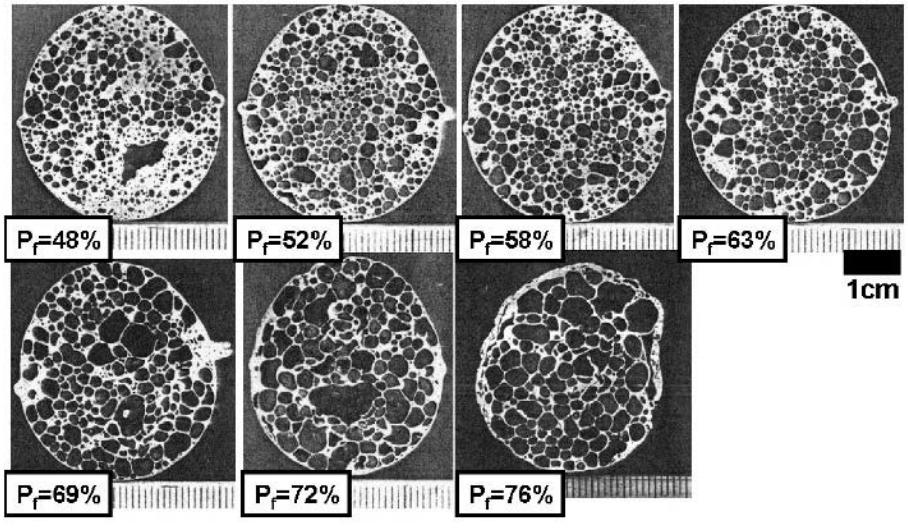

(b) Cross section of Al foam specimens

Fig. 5—Morphology of 6061 Al foams fabricated for variation of the porosity fractions: (*a*) surface appearances of 6061 Al foam specimens and (*b*) cross section of Al foam specimens.

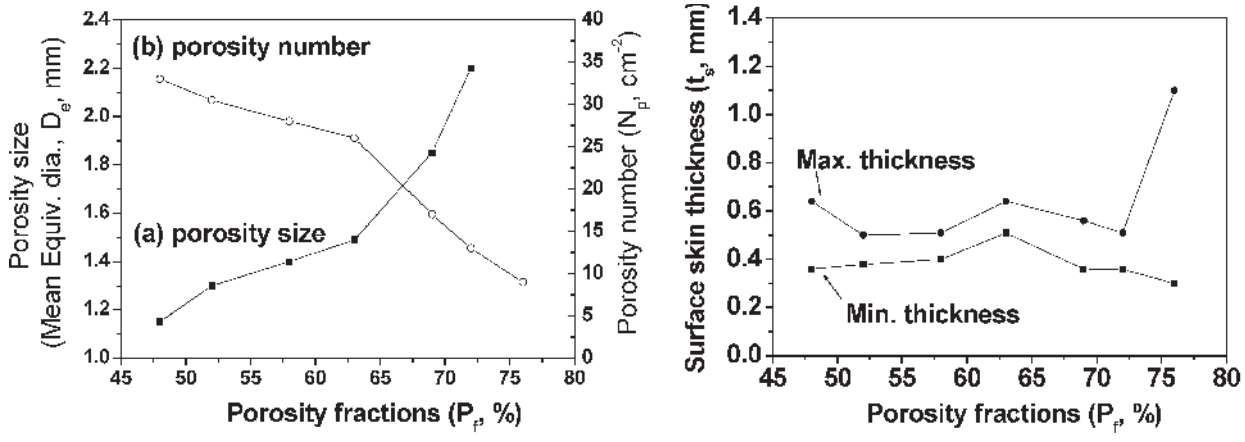

Fig. 6—Relationship between porosity fractions and morphological properties such as (*a*) porosity size, (*b*) porosity number, and (*c*) surface skin thickness.

is lower, cell walls become thick and deformation behavior occurs, as in bulk solid material. In addition, it has been reported that the mechanical properties of Al foam can be affected by flaws, the morphological rules of porosity, the regular deformation band, or nonuniform porosity distribution.[15] For the example of Figure 7(f), during initial deformation, the stress increases linearly with the strain increase by the elastic deformation of cell walls, and then the stress decreases slightly in accordance with the strain increase as the yield or fracture of cell walls is generated to $\varepsilon = 0.02$. From $\varepsilon = 0.05$, while stress decrease by buckling of cell walls and stress increase by plastic deformation of the specimen occur simultaneously, with the increase of strain, the stress remains almost steady. From $\varepsilon = 0.58$, the stress increases rapidly by densification of the specimen with strain increase, as the buckling or yield of cell walls is completed.

Figure 8 shows a cross-sectional area of the foam after the compression experiment. Deformation behavior due to bending and buckling of porosity is observed because a wrought alloy is used as the matrix alloy, whereas fracture

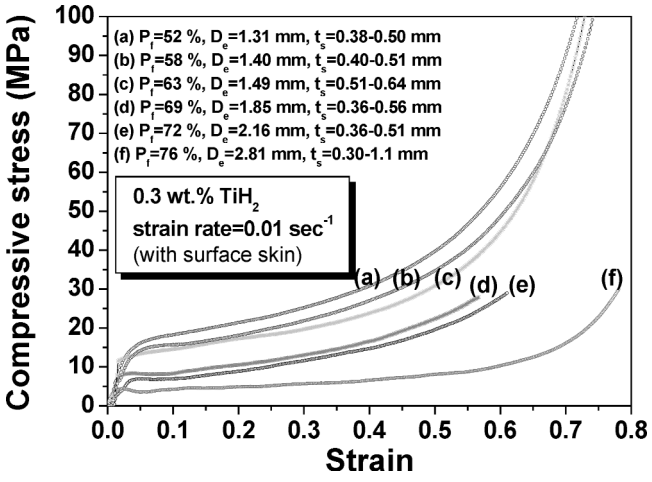

Fig. 7—Relationship between compressive stress and strain for 6061 Al foams with various porosity fractions.

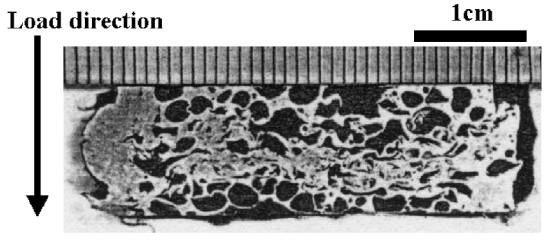

Fig. 8—Cross section of 6061 Al foam with 69 pct porosities after compression test (height reduction 80 pct).

is hardly observed. Also, it can be observed that the deformation is centralized with a sin curve shape in the direction of the height of the specimen. This shows that the size of the porosity in the specimen and the thickness distribution of cell walls are not uniform.

In order to investigate energy absorption characteristics according to the fraction of porosity, the energy absorption capacity (C) and efficiency ($E(\varepsilon)$) were calculated. These were calculated according to the following formulas:[4]

$$C = \int_0^{\varepsilon_m} \sigma d\varepsilon \qquad [1]$$

where C is the energy absorbed by foamed metal, σ is stress, and ε is strain); and

$$E(\varepsilon) = \frac{\int_0^{\varepsilon_m} \sigma d\varepsilon}{\delta\varepsilon} \qquad [2]$$

where $E(\varepsilon)$ is energy absorption efficiency.

Figures 9 and 10 show the variation of energy absorption capacity (C, MJ/m^3) with the porosity fraction (P_f) and the porosity size (D_e), respectively. It is observed that energy absorbed by the specimens decreased with an increase of both porosity fractions and porosity size. Also, this tendency was more easily observed in the case of higher strain.

Figure 11 shows the calculated energy absorption efficiency ($E(\varepsilon)$) using the compressive stress-strain curve of Figure 7. As can be seen from Figures 11(a) through (e), energy absorption efficiency decreases after initially increasing

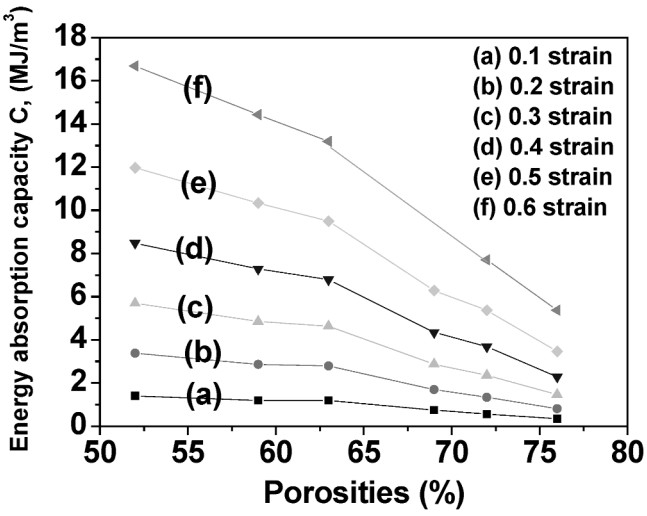

Fig. 9—Energy absorption capacity (C) of 6061 Al foams as a function of porosity fractions (P_f).

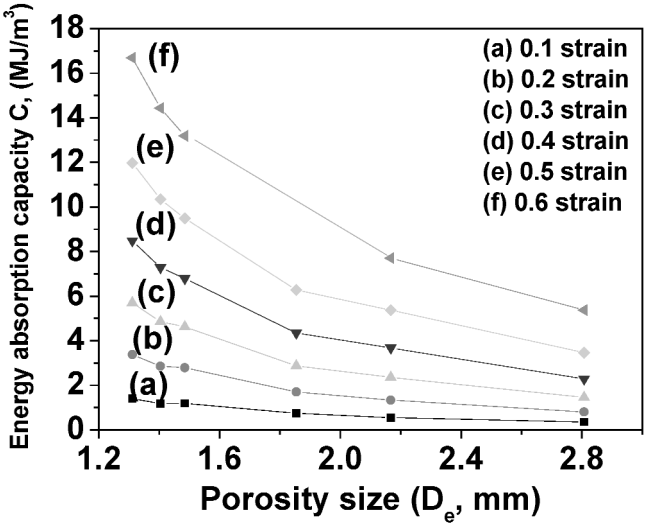

Fig. 10—Energy absorption capacity (C) of 6061 Al foams as a function of porosity size (D_e).

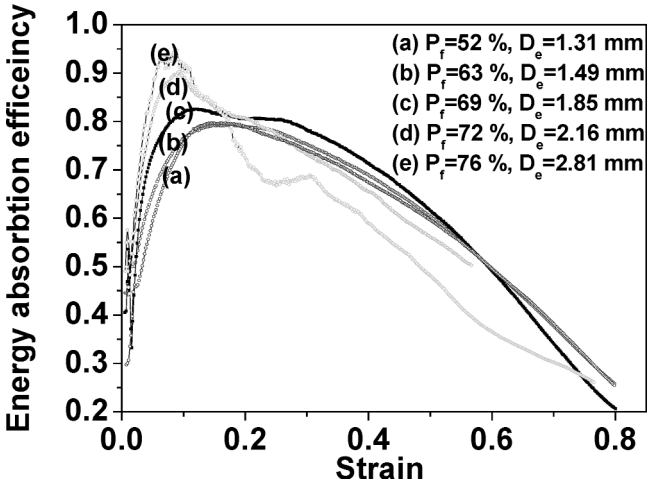

Fig. 11—Energy absorption efficiency ($E(\varepsilon)$) of 6061 Al foams as a function of porosity fractions.

with the strain increase. In addition, it can be seen that the peak value of energy absorption efficiency is proportional to the porosity fraction. For P_f = 52, 63, and 69 pct, the energy absorption efficiency-strain curve shows a wide and slow peak zone in comparison with P_f = 72, 76 pct. In the case of P_f = 76 pct (Figure 11(e)), the energy absorption efficiency remains steady after decreasing rapidly with strain increases in the range of ε = 0.2 to 0.3. As observed in Figure 5(b), it is estimated that the existence of the local nonuniform area could be one of the possible reasons.

B. *Effect of Surface Skin Thickness on Plateau Stress*

Surface skin that is generated inevitably when an Al foam product is produced significantly affects the mechanical properties. Comparing two Al foam products with the same relative density, the product with the surface skin has a much more regular and longer plateau stress area than that without the surface skin.[7,8] In this research, two 6061 Al foam specimens with almost the same morphological properties (porosity fraction, porosity size, and porosity number per unit area) except surface skin thicknesses were fabricated to investigate the effect of surface skin thickness on plateau stress (Figure 12). The measured morphological properties of specimens are shown in Table V.

Figure 13 shows the results after the compression experiment. The specimen with the thick surface skin (Figure 13(b)) shows a much longer and flatter plateau stress sector, but both specimens had the same compressive strength. It is estimated that there is distortion on the skin surface; however, this does not significantly affect the mechanical properties.

C. *Strain Rate Sensitivity of Al Foam Products with Low Porosities*

One of the most important general application fields for metallic foam is energy absorption, owing to their low rebound in dynamic crash situations and much higher strength than that of polymer foam.[6,8,16] In order to be used for energy absorption, the sensitivity of the plateau stress should be low in response to the strain rate. A lot of research has reported that the plateau stress of commercial closed-cell Al foam that has a volume of porosities over 70 pct is not significantly affected by a variation of the strain rate (<1 m/s).[6] However, studies on the strain-rate sensitivity of Al foam materials with porosity volume fraction lower than 70 pct. In order to investigate how variation of the strain rate affects the mechanical properties of low porosity fraction 6061 Al foam, two specimens with the same fraction porosity were fabricated using the fraction of porosity (pct)–final heating temperature (T_{a3}) diagram from Figure 3.

Figure 14 shows specimens that were used for a compression experiment. A specimen was produced in the same process as that shown in Figure 5. The morphological data of the specimens are shown in Table VI. The difference of porosity fraction among the specimens was approximately 1 pct. In addition, the differences of porosity size, number per unit area, and surface skin thickness among the specimens were negligible. The experiments were conducted under the condition of a strain rate between 10 and 0.01 s^{-1}.

Figure 15 shows stress-strain curves of 6061 Al foam obtained through the stress-strain curve compression experiment. For the 59 and 66 pct porosity fractions no significant difference was observed in compression strength or length and slope of plateau stress. (Figures 15(c) through (f)). However, for P_f = 52 pct, the strain rate of 10 s^{-1} shows approximately 5 MPa higher compressive strength in comparison with 0.01 s^{-1}.

For comparison with Al foam material, the strain-rate sensitivity of raw A365 Al alloys that were not foamed was investigated. Figure 16 shows the stress-strain curves with the variation of the strain rate of A356 Al material. There was no observable variation of the stress-strain curve with

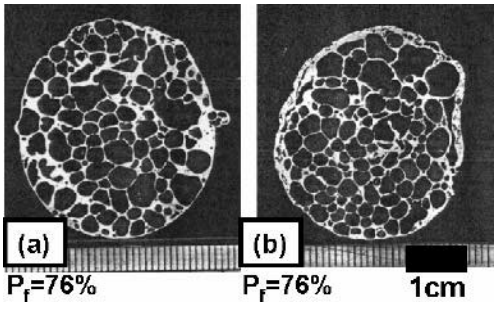

Fig. 12—6061 Al foams with different surface skin thickness (t_s): (*a*) 0.29 to 0.58 mm and (*b*) 0.30 to 1.0 mm.

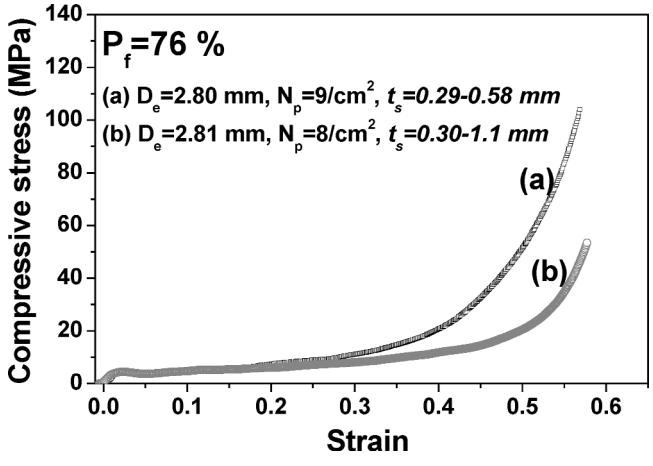

Fig. 13—Effect of the surface skin thickness on the plateau stress.

Table V. Morphological Properties of the Specimens in Figure 12

Specimen	Properties			
	Porosity Fractions (P_f, pct)	Porosity Size (D_e, mm)	Number per Unit Area (N_p, cm^2)	Surface Skin Thickness (t_s, mm)
Fig. 12(a)	76	2.80	9	minimum: 0.29, maximum: 0.58
Fig. 12(b)	76	2.81	8	minimum: 0.30, maximum: 1.10

the variation of the strain rate, which is consistent with what is known to be the general truth.

IV. CONCLUSIONS

The following conclusions from the evaluation of the mechanical properties of 6061 Al foam material could be obtained by applying the powder metallurgical and induction heating method.

1. With the increase of the porosity fractions (P_f = 48, 52, 58, 63, 69, 72, 76), the porosity diameter (D_e) increased

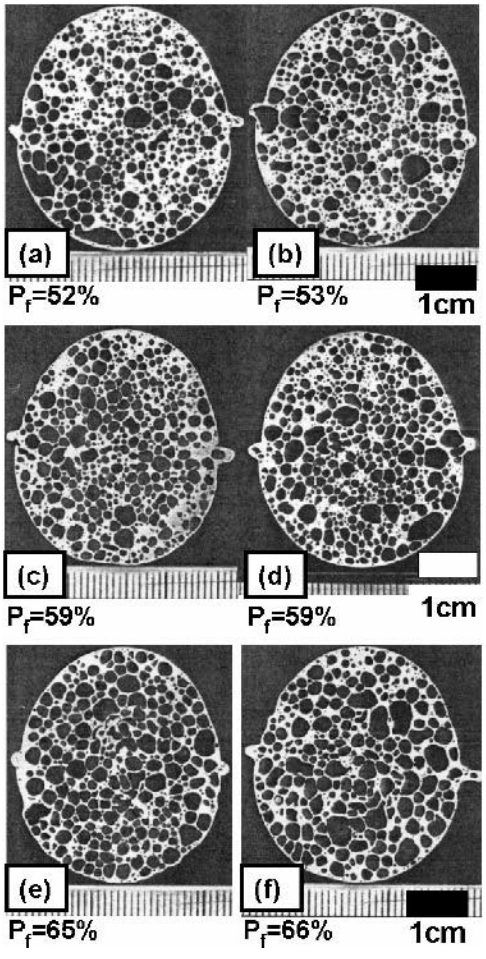

Fig. 14—(*a*) through (*f*) 6061 Al foams with various porosity fractions.

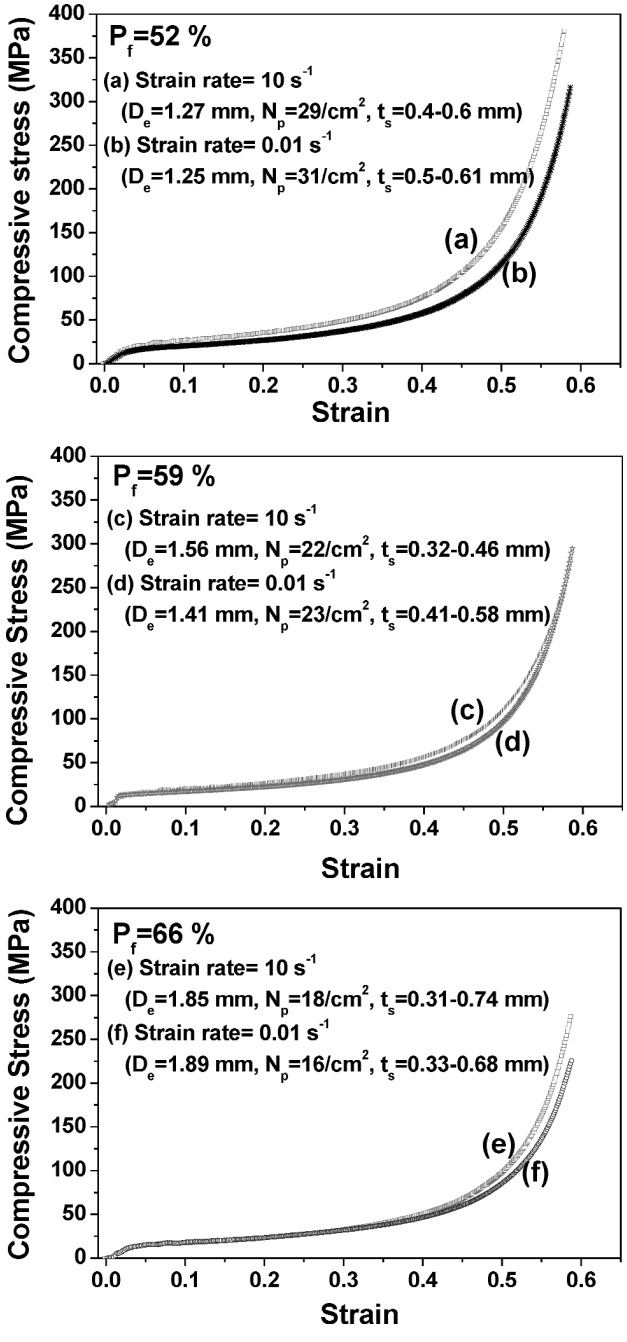

Fig. 15—Stress-strain curves for foamed 6061 alloy with various porosity fractions at two strain rates.

Table VI. Morphological Properties of the Specimens in Figure 14

Specimen	Properties			
	Porosity Fractions (P_f, Pct)	Porosity Size (D_e, mm)	Number per Unit Area (N_p,/cm^2)	Surface Skin Thickness (t_s, mm)
Fig. 14(a)	52	1.27	29	minimum: 0.4, maximum: 0.6
Fig. 14(b)	53	1.25	31	minimum: 0.5, maximum: 0.61
Fig. 14(c)	59	1.56	22	minimum: 0.32, maximum: 0.46
Fig. 14(d)	59	1.41	23	minimum: 0.41, maximum: 0.58
Fig. 14(e)	65	1.85	18	minimum: 0.31, maximum: 0.74
Fig. 14(f)	66	1.89	16	minimum: 0.33, maximum: 0.68

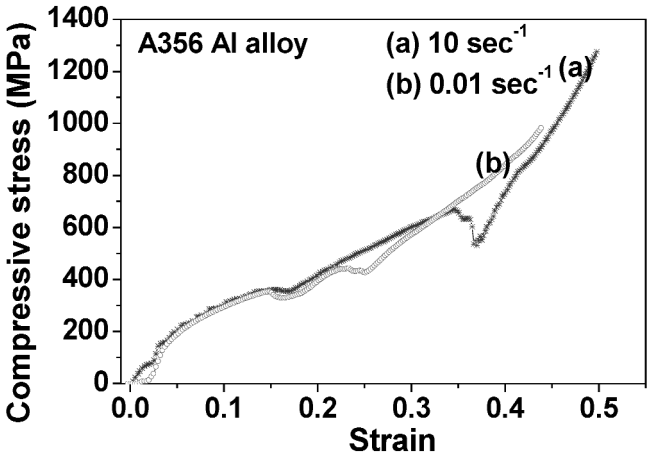

Fig. 16—Stress-strain curves of raw A356 Al alloys with different strain rates.

(D_e = 1.31, 1.40, 1.49, 1.85, 2.16, 2.81 mm) and the number per unit area of porosities (N_p) decreased (N_p = 33, 31, 28, 26, 17, 13/cm^2) due to both growth and coalescence of porosities. Even though the P_f, D_e, and N_p remarkably changed, the surface skin thickness (t_s) did not change. Over the P_f = 48 to 72 pct range, the t_s was maintained at about 0.4 to 0.6 mm. However, in the case of P_f = 76 pct, the t_s range remarkably increased to 0.3 to 1.1 mm.

2. In the case of 6061 Al foam with P_f = 52 to 76 pct, the compressive strength was decreased and the plateau stress area in the stress-strain curve was increased with increasing porosity fractions (P_f). It also could be seen that the energy absorption capacity (C) decreased with the increase of the porosity fraction, which tends to increase with increasing the porosity fraction (or porosity diameter). In addition, the energy absorption efficiency was maximized in the sector of strain between 0.1 and 0.2.
3. Through the compression experiment using two 6061 Al foam specimens with almost the same morphological properties (P_f = 76 pct, D_e = 2.8 mm, N_p = 9/cm^2) except surface skin thicknesses, the following was found. With the increase of the surface skin thickness, the plateau stress area increased, whereas the compressive strength was not changed.
4. In the case of 6061 Al foam of the porosity fractions, for the P_f = 59, 66 pct specimens, the strain rate sensitivity was very low, but for the P_f = 52 specimen, the strain rate of 10 s^{-1} showed an approximately 5 MPa higher compressive strength in comparison with 0.01 s^{-1}.

ACKNOWLEDGMENT

This work was supported by the National Research Laboratory (NRL) program of the Korean Ministry of Science and Technology (KMOST). The authors express their deep gratitude to the KMOST for financial assistance.

REFERENCES

1. A.G. Evans, J.W. Hutchinson, and M.F. Ashby: *Progr. Mater. Sci*., 1999, vol. 43, pp. 171-221.
2. F. Simancik: in *Metal Foams and Porous Metal Structures (MetFoam '99)*, J. Banhart, M.F. Ashby, and N.J. Fleck, eds., MIT Verlag, Berlin, Germany, 1999, pp. 235-40.
3. K.E. Geyer: in *Cellular Metals and Metal Foaming Technology (MetFoam 2001)*, J. Banhart, M.F. Ashby, and N.J. Fleck, eds., MIT Verlag, Berlin, Germany, 2001, pp. 31-36.
4. B. Wang, D.P. He, and G. Shu: in *Cellular Metals and Metal Foaming Technology (MetFoam 2001)*, J. Banhart, M.F. Ashby, and N.J. Fleck, eds., MIT Verlag, Berlin, Germany, 2001, pp. 351-54.
5. C.J. Yu, T.D. Claar, H.H. Eifert, I.W. Hall, R.E. Franz, K.T. Leihton, and D.F. Hasson: in *Metal Foams and Porous Metal Structures (MetFoam '99)*, J. Banhart, M.F. Ashby, and N.J. Fleck, eds., MIT Verlag, Berlin, Germany, 1999, pp. 235-40.
6. M.F. Ashby, A. Evans, N.A. Fleck, L.J. Gibson, J.W. Hutchinson, and H.N.G. Wadley: *Metal Foams—A Design Guide*, Butterworth-Heinemann, Berlin, Germany, 2000.
7. F. Simansik, J. Kovacik, and N. Minarikova: *Proc. 1998 PM World Congr. on Porous Materials*, Granada, Spain, European Powder Metallurgy Association (ZPMA), Old Bank Buildings, Belltone, Shrewsbury, UK. 1998, pp. 245-50.
8. L.J. Gibson and M.F. Ashby: in *Cellular Solids—Structure and Properties*, D.R. Clarke, S. Suresh, I.M. Ward, and M. Ashby, eds., 2nd ed., Cambridge University Press, Cambridge, United Kingdom, 1997.
9. R. Kresse: in *Metal Foams and Porous Metal Structures (MetFoam '99)*, J. Banhart, M.F. Ashby, and N.J. Fleck, eds., MIT Verlag; 1999, pp. 109-12.
10. A.R. Kennedy: *Scripta Mater*., 2002, vol. 47, Vienna University of Technology, pp. 763-67.
11. V. Gergley and T.W. Clyne: in *Metal Foams and Porous Metal Structures (MetFoam '99)*, J. Banhart, M.F. Ashby, and N.J. Fleck, eds., MIT Verlag, Berlin, Germany, 1999, pp. 83-89.
12. I. Duarte and J. Banhart: *Acta Mater*., 2000, vol. 48, pp. 2349-62.
13. S.W. Youn, S.H. Lee, and C.G. Kang: *Proc. Inst. Mech. Eng. Part B–J. Eng. Manufacture*, 2003, vol. 217 (2), pp. 201-11.
14. J. Kovasik and F. Simansik: in *Deformation and Fracture in Structural PM Materials, DF PM '99*, L. Parilak and H. Danninger, eds., IMR SAS, Kosice, 1999, pp. 106-14.
15. S.K. Kim, T.W. Hong, S.H. Cho, and Y.J. Kim: *J. Kor. Foundrymen's So*., 1998, vol. 18 (5), pp. 419-25.
16. R. Gradinger, F. Simancik, and H.P. Degischer: *Welding Technol., Mater. Mater. Testing, Fract. Mech. Quality Management*, 1997, vol. 2, pp. 701-12.